

Electronic Supplementary Information

Fabrication of Prime Number Checkers Based on Colorimetric Responses of Gold Nanoparticles

Zhenzhen Huang, Bohui Duan, Jinshuo Li, Min Wang, and Wensheng Yang*

State Key Laboratory of Inorganic Synthesis and Preparative Chemistry, College of
Chemistry, Jilin University, Changchun 130012, P. R. China

E-mail: wsyang@jlu.edu.cn

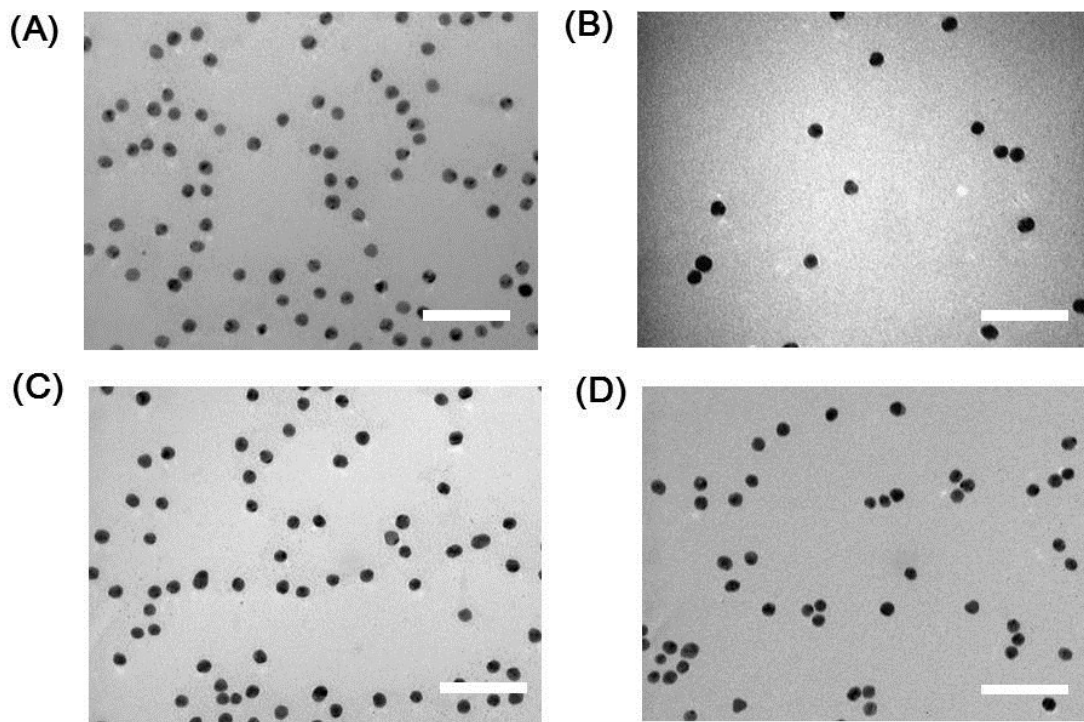


Fig. S1 TEM images of (A) Au NPs, (B) Au-Cys-5, (C) Au-Cys-10 and Au-Cys-50. The scale bars were 100 nm. Average size of the citrate-capped, quasi-spherical Au NPs were 15 nm, which kept unchanged after the addition of 5, 10 and 50 μM of Cys.

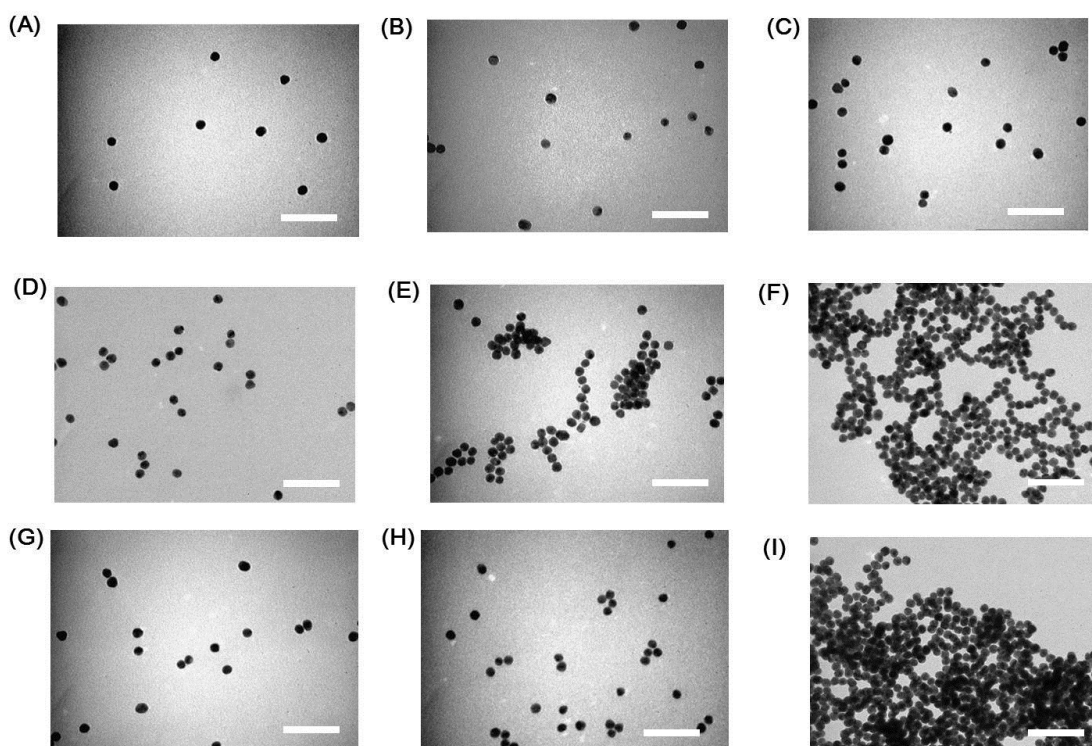


Fig. S2 (A–C) TEM image of Au -Cys-5 after the addition of (A) 5, (B) 10 and (C) 50 μM of Hg^{2+} . (D–F) TEM image of Au -Cys-10 after the addition of (D) 5, (E) 10 and (F) 50 μM of Hg^{2+} . (G–I) TEM image of Au -Cys-50 after the addition of (G) 5, (H) 10 and (I) 50 μM of Hg^{2+} . The scale bar represents 100 nm. No aggregation was observed for the Au-Cys-5 upon the addition of 5–50 μM Hg^{2+} . The Au-Cys-10 kept well dispersed after the addition 5 μM of Hg^{2+} , became moderately aggregated in the presence of 10 μM of Hg^{2+} , and underwent extensive aggregation upon the addition of 50 μM Hg^{2+} . For the Au-Cys-50, no obvious aggregation was identified in presence of 5–10 μM Hg^{2+} and extensive aggregation was identified when the concentration of Hg^{2+} was elevated to 50 μM .

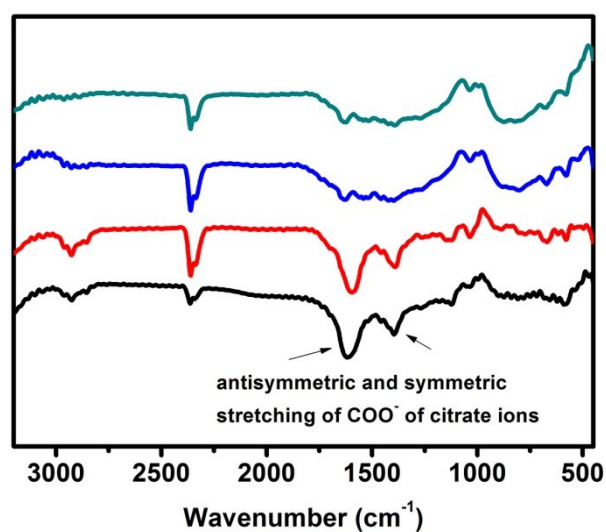


Fig. S3 FTIR spectra of the citrate-capped Au NPs (black), the Au-Hg²⁺-10 (red), the citrate-capped Au NPs after the addition of 10 μ M of Cys (blue) and the Au-Hg²⁺-10 after the addition of 10 μ M of Cys (green). The citrate-capped Au NPs present two characteristic peaks at \sim 1390 and \sim 1590 cm^{-1} , assigned to the symmetric and antisymmetric vibrations of COO⁻ of citrate (see Ref. 39 in the text), which almost kept unchanged after the addition of 10 μ M of Hg²⁺, indicating the co-existence of citrate and Hg²⁺ ions on the Au NP surface. When 20 μ M Cys was added into the citrated-capped Au NPs and Au-Hg-10, intensity of the peaks at \sim 1390 and \sim 1590 cm^{-1} decreased greatly, suggesting most of the citrate had been replaced by Cys either in presence or absence of Hg²⁺ ions. This is reasonable since the thiol group of Cys had much stronger affinity to Au than the carboxyl group of the citrate.

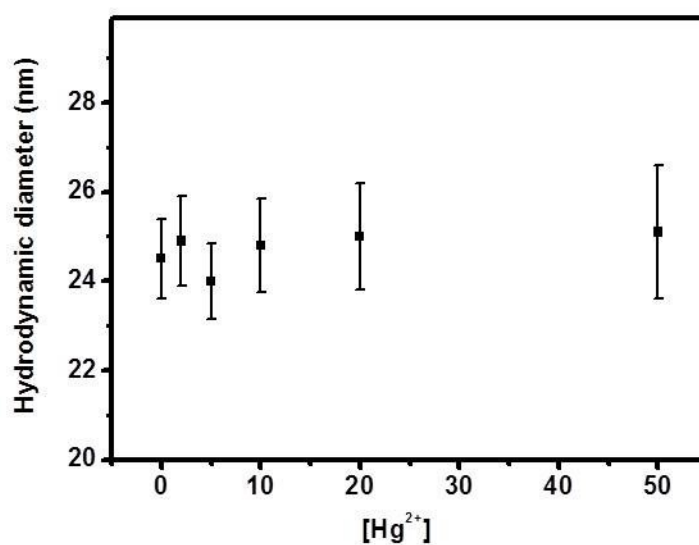


Fig. S4 Hydrodynamic diameter of the Au NPs recorded under different Hg²⁺ concentration. The diameter kept almost unchanged after the addition of 2, 5, 10, 20 and 50 μM Hg²⁺, implying that the Hg²⁺ tend to be adsorbed on the of the Au NP via a surface monolayer/submonolayer fashion.

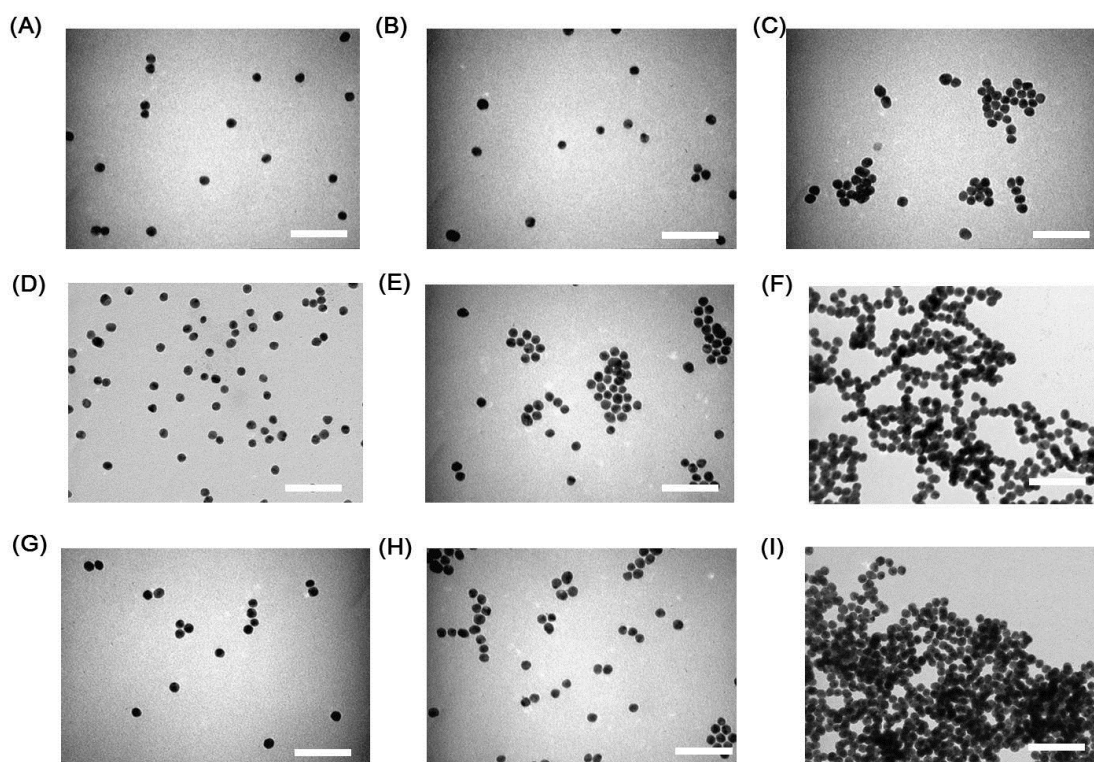


Fig. S5 (A–C) TEM images of the Au-Hg²⁺-5 upon the addition of (A) 0, (B) 10 and (C) 50 μM of Cys. (D–F) TEM images of Au-Hg²⁺-10 upon the addition of (D) 0, (E) 10 and (F) 50 μM of Cys. (G–I) TEM images of Au-Hg²⁺-50 upon the addition of (G) 0, (H) 10 and (I) 50 μM of Cys. The scale bar represents 100 nm. TEM observations showed that there was little change in size and shape of the citrate-capped Au NPs in presence of 5, 10 and 50 μM of Hg²⁺. The Au-Hg²⁺-5 and Au-Hg²⁺-50 only underwent aggregation at the high Cys concentration (50 μM), and the Au-Hg²⁺-10 underwent aggregation at the low Cys concentrations (10 μM).

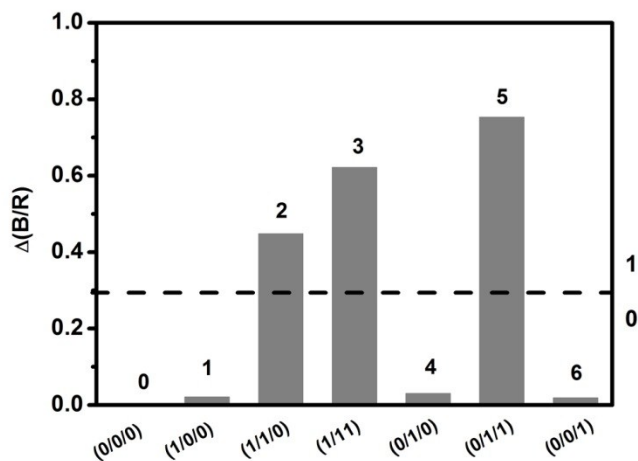


Fig. S6. (A) Change in the $\Delta(B/R)$ for 3-bit prime number checker. Photos of various Au NP dispersions of the 3-bit prime number checker were taken by a digital camera (Sony R1X, Fig. 4B). The photos were then processed by using a free RGB analysis software (Colorcop) for extracting the RGB variations. The color change of the checker can also be evaluated by RGB analysis. The intensity ratio of blue to red (B/R) channel (in RGB chroma) may serve as another logic output. The output is defined as “0” and “1” when $\Delta(B/R)$ (intensity ratio of (B/R) of various input strings minus that of (B/R) of the initial state) is lower and higher than 0.2, respectively. Only the input strings that encode prime numbers “2”, “3” and “5” can give rise to the output of 1. Such logic responses from RGB analysis were fully consisted with the truth table of 3-bit prime number checker (Fig. 4D), indicating the RGB signals can be used as another outputs of prime number checker besides A_{640}/A_{520} values and the color of Au NPs dispersions.

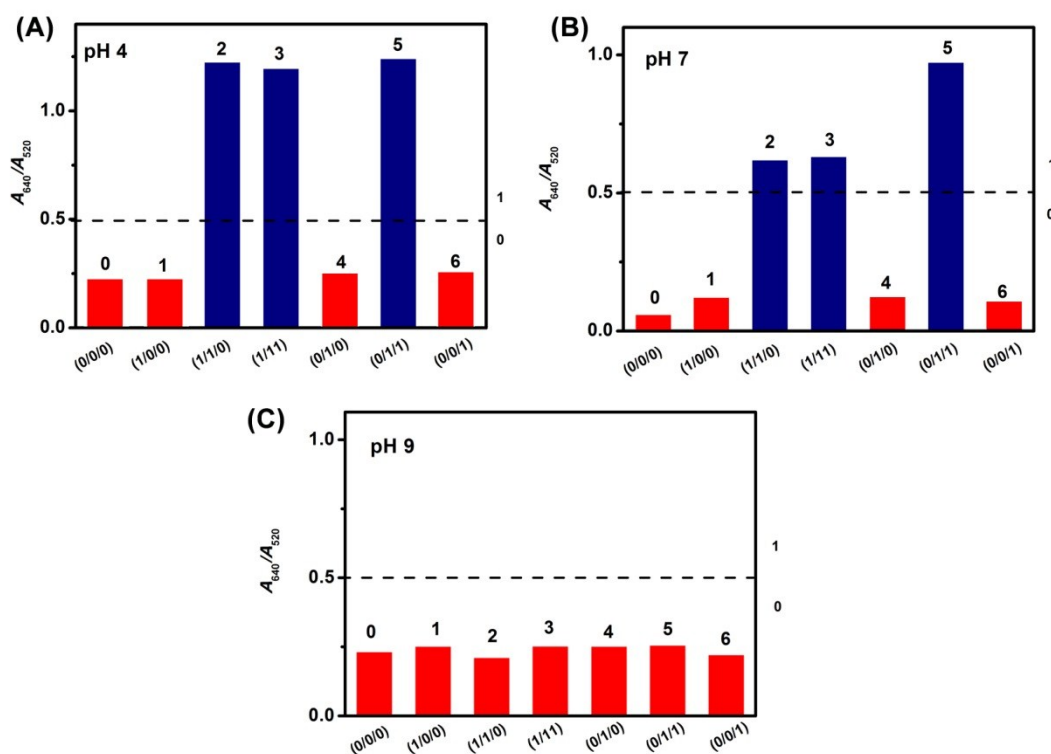


Fig. S7. The A_{640}/A_{520} values of the Au NPs recorded under the different inputs at pH (A) 4, (B) 7 and (c) 9. The pH of the original Au NPs solution (pH 5.5) was tuned to the desired value by using HCl or NaOH. The 3-bit prime number worked well under the acid and neutral pH (pH 4 and pH 7). However, the colorimetric change was notably suppressed under the alkaline pH (pH 9), since the hydrogen bonds between the first and second layers of Cys in Au-Cys-10 would be destroyed under the alkaline pH. Meanwhile, the promoted hydrolysis of Hg^{2+} ions at alkaline pH may also contributed to the suppressed aggregation.

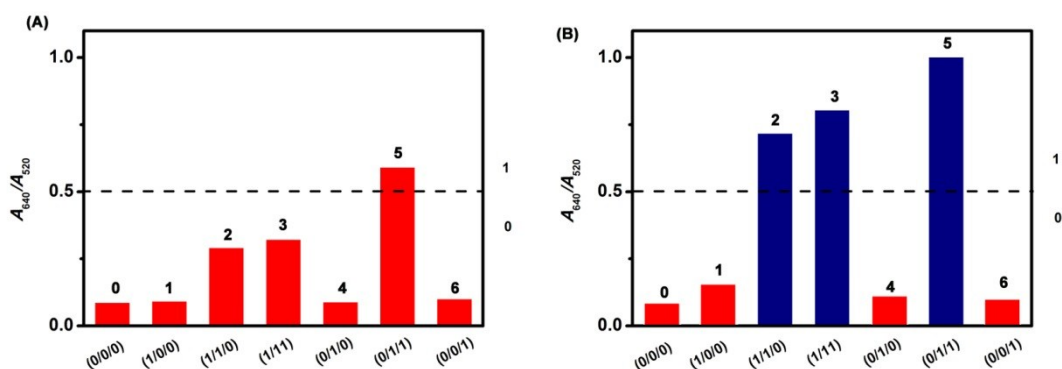
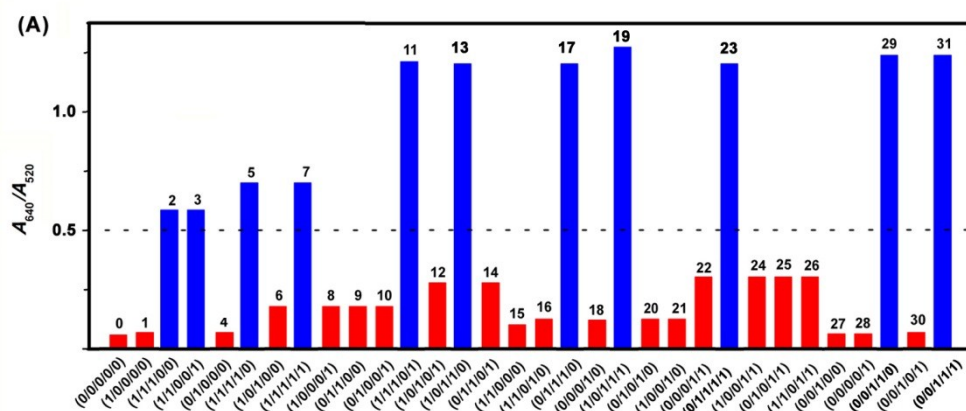


Fig. S8. The A_{640}/A_{520} values of 25 nm Au NPs recorded under the different inputs. (A) Input 1 (10 μM Cys), Input 2 (10 μM Hg^{2+}) and Input 3 (10 μM Cys). (B) Input 1 (20 μM Cys), Input 2 (10 μM Hg^{2+}) and Input 3 (20 μM Cys). The larger Au NPs (25 nm) failed to fabricate the 3-bit prime number checker by using the same inputs as the 15 nm Au NPs. When 20 μM of Cys was used as inputs, the colorimetric responses of the 25 nm Au NPs to Cys and Hg^{2+} inputs were consistent with the truth table of 3-bit prime number checker. This is reasonable since the 25 nm Au NPs require more Cys to achieve the bilayer adsorption of Cys on their surface.



(B)

Natural number	Input 1 5 μ M Cys	Input 2 5 μ M Cys	Input 3 10 μ M Hg ²⁺	Input 4 50 μ M Cys	Input 5 10 μ M Hg ²⁺	Output
0	0	0	0	0	0	0
1	1	0	0	0	0	0
2	1	1	1	0	0	1
3	1	1	0	0	1	1
4	0	1	0	0	0	0
5	1	1	1	1	0	1
6	1	0	1	0	0	0
7	1	1	1	1	1	1
8	1	0	0	0	1	0
9	0	1	1	0	0	0
10	0	1	0	0	1	0
11	1	1	1	0	1	1
12	1	0	1	0	1	0
13	1	0	1	1	0	1
14	0	1	1	0	1	0
15	1	1	0	0	0	0
16	1	1	0	1	0	0
17	0	1	1	1	0	1
18	0	0	0	1	0	0
19	1	0	1	1	1	1
20	0	1	0	1	0	0
21	1	0	0	1	0	0
22	0	0	0	1	1	0
23	0	1	1	1	1	1
24	1	0	0	1	1	0
25	0	1	0	1	1	0
26	1	1	0	1	1	0
27	0	0	1	0	0	0
28	0	0	0	0	1	0
29	0	0	1	1	0	1
30	0	0	1	0	1	0
31	0	0	1	1	1	0

Fig. S9. (A) Change in the A_{640}/A_{520} and (B) truth table for 5-bit prime number checker.

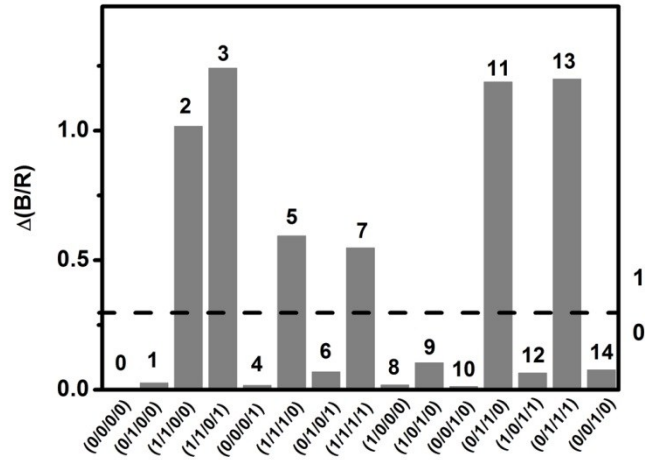


Fig. S10. (A) Change in the $\Delta(B/R)$ for 4-bit prime number checker. Only the input strings that encode prime numbers “2”, “3”, “5”, “7”, “11” and “13” can give rise to the output of 1. Such logic responses from RGB analysis were fully consisted with the truth table of 4-bit prime number checker (Fig. 5D).

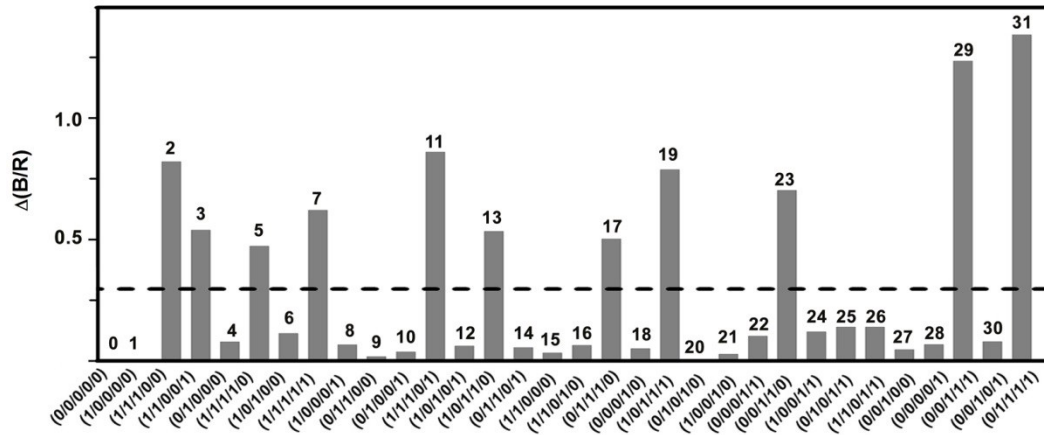


Fig. S11. (A) Change in the $\Delta(B/R)$ for 5-bit prime number checker. Only the input strings that encode prime numbers “2”, “3”, “5”, “7”, “11”, “13”, “17”, “19”, “23”, “29” and “31” can give rise to the output of 1. Such logic responses from RGB analysis were fully consisted with the truth table of 5-bit prime number checker (Fig. S9B).